Available online at www.sciencedirect.com
SCIENCE DIRECT®
Catalysis Today 89 (2004) 57–65
CATALYSIS TODAY
www.elsevier.com/locate/cattod

Dissociation of vibrationally excited methane on Ni catalyst Part 1. Application to methane steam reforming

Tomohiro Nozaki*, Nahoko Muto, Shigeru Kado, Ken Okazaki

Department of Mechanical and Control Engineering, Tokyo Institute of Technology, 2-12-1 O-okayama, Meguro-ku, Tokyo 152-8552, Japan

Abstract

This paper describes extensive experimental research on steam reforming of methane using barrier discharges with/without Ni/SiO_2 catalyst. Nickel catalyst clearly showed chemical activity at 400 °C in the presence of barrier discharge. Methane conversion largely exceeded over equilibrium conversion rate, whereas product selectivity tended to follow equilibrium composition at given temperature: energy cost and energy efficiency achieved 134 MJ/kg H_2 and 69%, respectively. Electric property was unchanged in the presence of nickel catalyst, but at least 400 °C must be maintained in order to derive synergistic effect between barrier discharge and Ni/SiO_2 catalyst. Methane activation mechanism is also discussed based on numerical simulation on streamer propagation in pure methane. Vibrationally excited methane is most abundant ($1016\,cm^{-3}$ at 300 K, 101.3 kPa) and long-lived ($\sim$1 μs) radical species produced by electron impact, and those vibrational species seemed to improve dissociative chemisorption on nickel surface at low temperature, leading to remarkable process improvement.

Keywords: Natural gas; Methane; Hydrogen; Steam reforming; Vibrational excitation; Low temperature catalysis; Energy saving; Environment; Barrier discharge

1. Introduction

Authors have for years been involved in natural gas conversion chemistry such as direct synthesis of methanol using barrier discharges [1–3]. Although industrial applications of C_1 chemistry depend mostly on catalytic conversion processes, plasma catalysis poses the following advantages that catalytic process cannot achieve. More recently, applications of plasma materials conversion are highlighted as promising technique for energy saving and environment safe purposes with increasing demand of hydrogen and synthesis gas [4–7].

1. Power resources and its cost (solar, wind, local power, etc.).
2. Non-equilibrium processing (independent of temperature and pressure).
3. Omission of redundant decontamination process such as desulfurization.
4. Co-production of valuable materials as carbon nanotube and graphite nano-particles.
5. Compactness and lightweight.
6. Rapid response.

The currently recognized biggest challenge is the improvement of energy cost and energy efficiency. From this point, authors performed numerical simulation on streamer propagation in pure methane to investigate fundamental electric and chemical processes for methane activation. According to numerical analysis, electrons tend to lose 40–50% of primary energy through vibrational excitation collisions. Population of vibrational methane (bending mode: 0.16 eV, stretching mode: 0.36 eV) reaches 100 times higher than electron density. Those enormous numbers of excited species cannot contribute further chemical reactions due to relatively low reactivity. On the other hand, vibrationally excited methane promotes dissociative chemisorption on a specific transition metal at lower temperature [8–10]. From these aspects, authors developed barrier-discharge enhanced catalytic-bed (BEC) reactor combined with 3 wt.% Ni/SiO_2 pellets for efficient decomposition of methane, and applied this technique to steam reforming. The rector scheme was first invented by Mizuno and coworkers [11,12], Yamamoto and coworkers [13,14], and Futamura and coworkers [7,15]. As a result, methane conversion, hydrogen selectivity, thus energy cost was greatly improved. This paper concentrates

* Corresponding author. Tel.: +81-3-5734-2179; fax: +81-3-5734-2893.
E-mail address: tnozaki@mech.titech.ac.jp (T. Nozaki).

0920-5861/$ – see front matter © 2003 Elsevier B.V. All rights reserved.
doi:10.1016/j.cattod.2003.11.040

on analyzing fundamental electric and chemical characteristics of plasma/catalyst hybrid system for methane steam reforming. Conventional dielectric barrier discharge (DBD) was also investigated at the same time to provide reference data, and synergistic effect between barrier discharge and catalyst is extensively discussed.

2. Methane activation by electron impact

2.1. Streamer formation and related chemistry

We performed numerical simulation on streamer propagation in pure methane for better understanding of elementary electronic and chemical processes [16]. Fig. 1 schematically represents various electronic and kinetic processes in streamer on an approximate time scale. The model consists of two different stages: streamer propagation and related chemistry where ionization, excitation, and dissociation of methane by electron impact were evaluated along with time evolution of field strength and electron density (2–3 ns). Complete set of cross-sections for methane was thoroughly reviewed by Morgan [17]. We adopted cross-section set compiled by Davies et al. [18] as recommended by Morgan because Davies provided detailed cross-section set over wide range of E/N along with experimental data ($50 < E/N < 1000$ Td (townsend units)). During streamer development, electric energy input and thus radical formation efficiency was analyzed in detail. After the termination of streamer development, the second stage, ionic and free radical chemistry that would last for 10 ms was performed with the reaction scheme proposed by Tachibana et al. [19]. Sixteen neutral species, four positive ions, and two vibrationally excited species were incorporated in our model. Temperature and pressure were 300 K and 101.3 kPa, respectively.

Fig. 2 illustrates the calculation domain along with boundary and initial conditions. We simulated anode directed streamer (ADS) ignited from tiny plasma spot located in front of the cathode. We assumed that streamer was one-dimensional cylinder with 100 μm diameter. Basic equations were continuity equations for electron, ions, and neutral species, and Poisson's equation. Thirty-eight elementary reactions including eight inelastic collisions were simultaneously solved. Physical modeling and mathematical

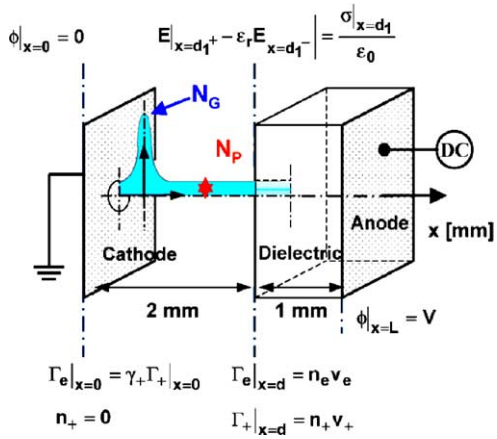

Fig. 2. Calculation domain and boundary and initial condition: $N_G = 107\,\mathrm{cm}^{-3}$, $N_P = 10^3\,\mathrm{cm}^{-3}$.

procedure are discussed in detail by Dhali and coworkers [20,21], Morrow and coworkers [22–24], and Braun and coworkers [25–27].

2.2. Radical formation and energy branching

Fig. 3 shows temporal development of radical species and final products. All radical species including electron are rapidly increases with streamer propagation. Electron density reaches $10^{14}\,\mathrm{cm}^{-3}$. C, CH, CH_2, and H are quickly disappeared after streamer termination to produce C_2H_2, C_2H_4, and H_2. CH_3 survives relatively long time, but gradually recombine to form C_2H_6. The most abundant species are vibrationally excited methane that reached 100 times higher than electron density. However, it cannot participate further reactions because of low reactivity. Therefore, production of vibrational methane leads to significant energy loss.

Energy spent by electrons to produce ith radical specie was calculated by the following equation:

$$w_i\,(\mathrm{J}) = s\int_{\mathrm{gap}}\int_0^{\tau} \varepsilon_i k_i N_e N_{\mathrm{CH_4}}\,\mathrm{d}t\,\mathrm{d}x \qquad (1)$$

Here s is the cross-section of cylindrical filament body (m^2), τ the streamer lifetime (s), ε_i the excitation threshold (eV), k_i the rate constant (m^3/s), N_e the electron density (m^{-3}), N_{CH_4} the methane density (m^{-3}). Approximate radical density and

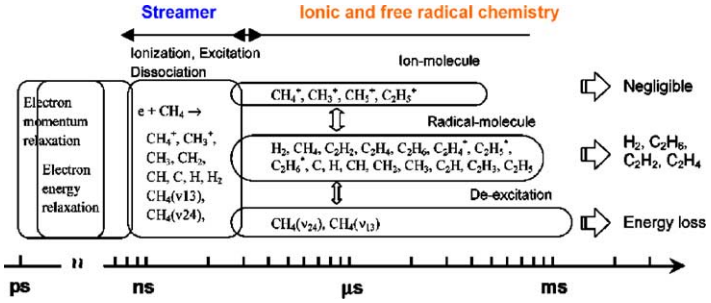

Fig. 1. Reaction scheme.

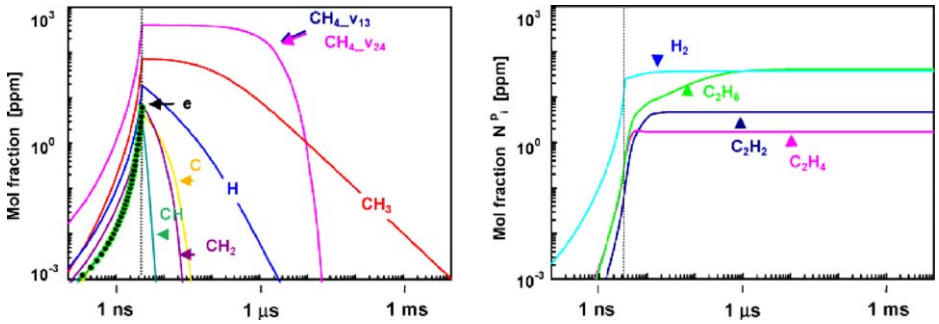

Fig. 3. Evolution of radical species and final products (200 Td, 101.3 kPa, 300 K): (a) Radical species; (b) final products.

Table 1
Electric processes and energy branching (20 Td, 101.3 kPa, 300 K, lifetime ≈ 3.5 ns, $N_e \approx 10^{14}$ cm^{-3})

Reaction (CH_4 + e)	ε_i (eV)	Density	Energy branch (%)	k_i/W_e[a] [cm^2] (500 Td)
→$CH_4(\nu 24)$ + e	0.162	$150N_e$	11.9	372 × 10^{-18}
→$CH_4(\nu 13)$ + e	0.361		24.5	316
→CH_3 + H + e	9.0	$10N_e$	17.0	88.4
→CH_2 + H_2 + e	10.0	$\sim N_e$	13.2	79.6
→CH + H_2 + H + e	11.0		10.8	71.5
→C + 2H_2 + e	12.0		9.3	64.5
→CH_4^+ + e + e	12.6	N_e	9.4	70.7
→CH_3^+ + H + e + e	14.3		4.0	46.6

[a] Drift velocity of electrons (cm/s).

energy distribution are summarized in Table 1 along with excitation threshold. Excitation threshold for vibrational excitation is of the order of 0.1–0.3 eV, however, 40% of input electric energy was consumed since rate constants are 10 times larger than other reactions. From this point, decomposition of vibrationally excited methane poses significant importance.

3. Experimental

3.1. Plasma–catalyst reactor and gas analysis

The experiment was performed based on two different barrier discharge reactors to clarify plasma–catalyst interaction. Fig. 4 shows the BEC reactor equipped with electric heater around external ground electrode. The wire-to-tube

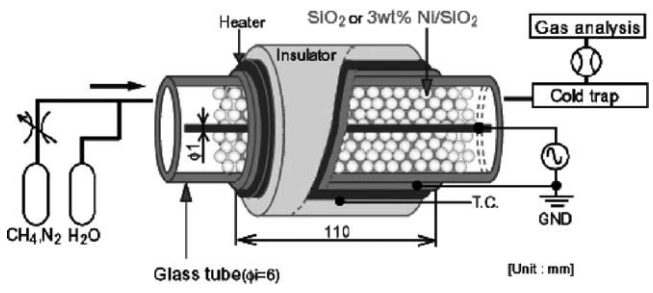

Fig. 4. Barrier-discharge enhanced catalytic-bed (BEC) reactor.

(ID 6 mm) reactor packed with 3 wt.% Ni/SiO_2 catalyst pellets (1.2 mm sphere) was located in a constant temperature bath where ambient temperature was kept constant at 120 °C to avoid liquid condensation. High voltage sine wave (76 kHz) was applied between wire and external electrode. The discharge was ignited at pellet contacts, and then propagated covering pellet surface. The void fraction of packed bed rector was 80% for 1.2 mm SiO_2 pellets. Methane and water-vapor mixture was fed into the reactor at various mixture ratio and flow rate. An amount of 10 vol.% nitrogen was included in methane cylinder as a reference for quantitative gas analysis. Reactor temperature was measured and controlled at the external electrode. The possible maximum temperature increase due to plasma itself was 210 °C at 16 W power input. The actual reaction temperature was increased up to 700 °C with external electric heater. Three different conditions were investigated in BEC reactor with (1) only 3 wt.% Ni/SiO_2 (without plasma), (2) plasma and 3 wt.% Ni/SiO_2, and (3) plasma with SiO_2 (without catalyst).

In addition, conventional DBD reactor given in Fig. 5 was used to provide reference data, and electric and chemical properties for barrier discharge were compared to results obtained in BEC reactor. The empty wire-to-tube reactor cannot be used for this purpose since wire electrode tended to reach red-hot due to its small heat capacity. This situation resulted in unstable plasma operations. High temperature wire electrode may act as a hot spot, leading to unexpected high reactivity for given temperature. Detailed experimental conditions were summarized in Table 2.

Table 2
Experimental conditions

I (DBD[a])	II (DBD + SiO_2)	III (DBD + 3 wt.% Ni/SiO_2)	IV (3 wt.% Ni/SiO_2)
Co-axial parallel	Packed-bed tubular		
0.5, 1.0 mm gap	SiO_2 pellet (200 m^2/g): 1.2 mm at 80% void		
2–10 (*S/C*)	Total flow rate: 25 and 33 sccm; 2–3 (*S/C*)		
10–90 W	Frequency: 10, 76 kHz; input power: 5–26 W		
10–300 sccm	120–400 °C	200, 400, 600, 700 °C	
165–400 °C	–	3 wt.% Ni/SiO_2, incipient-wetness	
1–76 kHz	–	3 wt.% Ni/SiO_2, incipient-wetness	

[a] Dielectric barrier discharge.

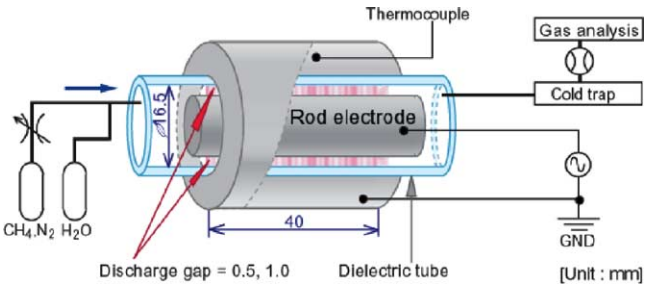

Fig. 5. Co-axial dielectric barrier discharge (DBD) rector.

Part of reaction gas was sampled after cold trap. H_2 and N_2 were analyzed by gas chromatograph equipped with TCD detector, and hydrocarbons such as CH_4, C_2 (mainly ethane), C_3 (propane) were measured by GC (FID). CO and CO_2 were also measured by GC (FID) after methanation.

4. Results and discussion

4.1. Electric properties for DBD and BEC rector

Fundamental electric properties for individual reactor have been analyzed based on steady state discharge model. This model provides time- and space-averaged electric properties of barrier discharges and commonly used for macroscopic characterization purpose. This model is expressed by the following relation:

$$\overline{N_e}\,(m^{-3}) = \frac{\kappa}{eN\overline{V_e}}\frac{\bar{W}}{(\bar{E}/\bar{N})Sd} \quad (2)$$

Here κ is the part of energy carried by electrons. Generally assumed to be 0.5 for streamer type breakdown (–), W the discharge power (W), S the electrode area (cm^2), d the gap (cm), e the elementary charge (C), E/N the reduced field strength (Td($= 10^{-17}$ V cm^2)), V_e the drift velocity of electron (cm/s) and N the molecular density (cm^{-3}). Discharge power and reduced field strength was derived from Lissajous figure, and electron drift velocity was calculated by ELENDIF software incorporated with cross-section data provided by Davies et al. [18] for methane and Hayashi [28] for water-vapor, respectively. ELENDIF calculates time-dependent electron energy distribution function by two-term spherical harmonic expansion solutions of Boltzmann transport equation. Swarm parameters derived by the solution provide satisfactorily good agreement when reduced field strength was lower than 500 Td [18,29].

Fig. 6 shows time- and space-averaged electron density against average field strength. Hollow symbol represent DBD reactor, whereas solid symbol represent BEC reactor, respectively. DBD reactor demonstrates typical negative differential conductive (NDC) characteristics, showing that high field strength and high electron density cannot be simultaneously attained. Two horizontal doted lines showed constant power line. Discharge power and electron density increases non-linearly with respect to operating frequency, and reduced field strength approaches breakdown field in pure methane (83 Td). It is interesting to note that average field strength exceeded breakdown field when operating frequency was low enough. This situation is also found in computer simulation: the actual field strength at streamer head, where the copious amount of radical species are produced, generally exceed breakdown filed [25–27]. It is suddenly reduced with increasing frequency, and approaches breakdown field in pure methane probably due to increase in ions remaining between gap.

In the case of BEC reactor, situation became even more complicated because discharge would be ignited at pellet contacts, and propagates along pellet surface. However, discharge characteristics also show typical NDC characteristics. Reduced field strength was approximately near breakdown

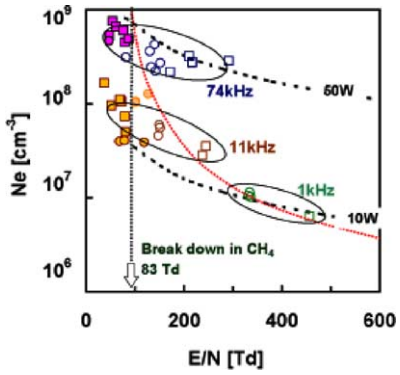

Fig. 6. Electric properties based on steady state discharge model. Hollow symbols represent DBD reactor: (○) 1.0 mm gap, (□) 0.5 mm. Solid symbols are BEC: (●) SiO_2, (■) Ni/SiO_2.

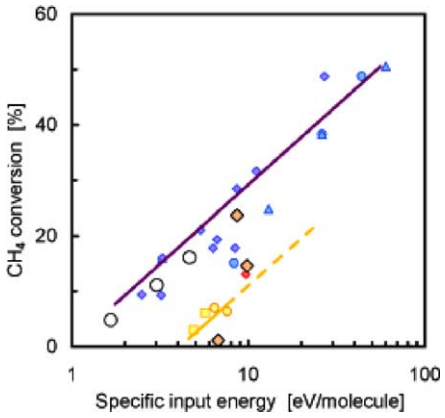

Fig. 7. Methane conversion vs. specific input energy. The results were obtained without nickel catalyst. Wide ranges of conditions as listed in Table 2 (I and II) were examined.

field of methane at high frequency operation. There was not remarkable difference with respect to reactor configuration, operating conditions, and the presence of nickel catalyst.

4.2. Methane conversion by barrier discharge

Methane conversion property in DBD reactor was investigated without nickel catalyst. Fig. 7 shows the methane conversion with respect to specific input energy. All data were obtained in DBD and BEC reactors in wide ranges of conditions as described in Table 2 (I and II). Methane conversion is monotonically increases with specific input energy. The same as electric properties, various parameters such as gas composition, reaction temperature, frequency dose not affect reaction characteristics. The more input energy resulted in more methane conversion, and energy efficiency was about 0.2–0.6% (Eq. (4)) regardless of operating conditions.

Fig. 8(a) and (b) shows the product selectivity plotted against specific input energy. The selectivity for all products is also expressed by a single parameter, i.e. specific input energy. Ethane (C_2) was first produced by CH_3 coupling, then propane (C_3) and butane (C_4) was successively produced by secondary reaction of C_2 and C_3 products. Combined selectivity for those products amounted to 40% over 10 eV/molecule. $\Delta H_2/\Delta CH_4$ ratio, i.e. hydrogen selectivity, is ideally between 3 and 4 for steam reforming of methane, but actual selectivity was limited by 2.5 since 40% of methane turned into C_2 and C_3 hydrocarbons. In addition to hydrogen, carbon monoxide was dominant product. Water–gas-shift reaction would be negligible due to low temperature reforming. Operating conditions showed little impact on product selectivity, and carbon oxides also reached constant value at higher input energy. A little amount of alcohol such as methanol and ethanol was detected, but selectivity was below 1% when specific input energy exceeded 10 eV/molecule.

4.3. Barrier-discharge enhanced catalytic process

Methane reforming in BEC reactor was performed to investigate combined effect of barrier discharge and 3 wt.% Ni/SiO_2 catalyst. SiO_2 pellet (1.2 mm) was filled at 80% void fraction. Reaction temperature was increased up to 700 °C by external electric heater. Gas composition, power input, and other conditions are already listed in Table 2. Catalyst bed was immersed in hydrogen atmosphere and maintained at 600 °C for 1 h before experiment. Fig. 9 shows the methane conversion characteristics for BEC reactor (line "A"). The results indicated by line "B" correspond to those obtained in DBD reactor. Methane conversion is remarkably promoted in BEC reactor when bed temperature was 600 °C. In addition, product selectivity was dramatically improved by combining barrier discharge and nickel catalyst. Characterization of reaction enhancement and its mechanism will be discussed by focusing on chemical equilibrium basis.

4.4. Synergistic effect between barrier discharge and catalyst

Fig. 10 compares the methane conversion characteristics for three different reaction systems. Results obtained by DBD reactor (without catalyst: I) and Ni/SiO_2 catalyst (with-

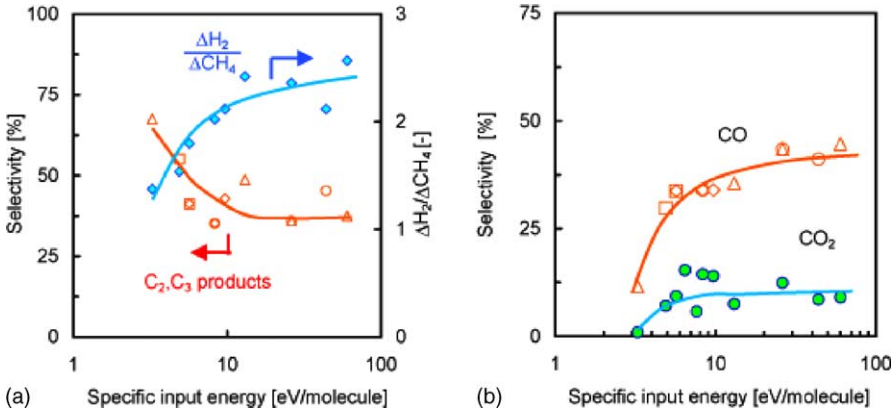

Fig. 8. Product selectivity of: (a) hydrogen, C_2, and C_3 components; (b) carbon oxides. The results were obtained without nickel catalyst. Conditions are listed in Table 2 (I and II).

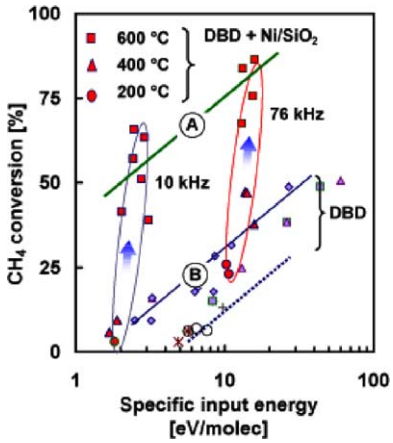

Fig. 9. Methane conversion: (A) barrier discharge + nickel catalyst; (B) barrier discharge.

out plasma: IV) are also plotted. Dotted line indicates equilibrium conversion at given temperature when $H_2O/CH_4 = 2$.

Barrier discharge is able to decompose methane at lower temperature, and 25% conversion was achieved at 200 °C. This is the great benefit of barrier discharges over catalytic reaction. However, methane activation by electron impact was almost independent of reaction temperature since electric property was not influenced by ambient temperature as shown in Fig. 6. As a result, methane conversion showed constant value until 400 °C [30]. When the temperature exceeded 400 °C, solid carbon or soot was gradually accumulated, and stable filamentary barrier discharge could not be maintained. We did not observe specific increase in methane conversion, whereas selectivity for propane and butane decreased. Methane is hardly decomposed even 900 °C in the absence of catalyst [31,32]. In fact, Mutaf-Yardimci et al. [33] applied pulsed corona discharge to preheated CH_4/CO_2/air mixture for hydrogen generation; however, a fraction of methane was pyrolized even at 900 °C, and

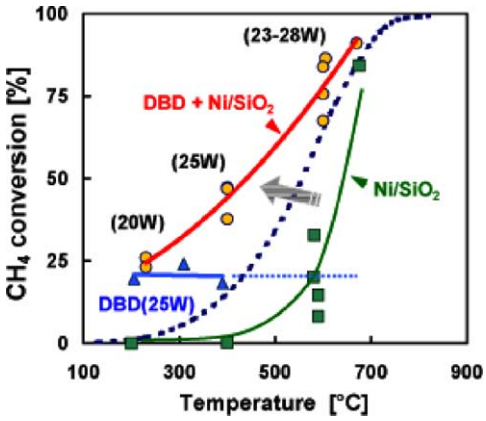

Fig. 10. Methane conversion characteristics. (▲): Barrier discharges (I), (■): 3 wt.% Ni/SiO_2 (IV), (●): DBD with 3 wt.% Ni/SiO_2 (III), (- - -) equilibrium conversion ($H_2O/CH_4 = 2$). Discharge power: 20–30 W, residence time: 1.0 s, frequency 76 kHz.

synergistic effect could not be observed when the plasma was combined. The addition of air prevented the formation of soot, but 30–40% of synthesized hydrogen turned into water in their experiment. So long as methane dissociation relies only on electron impact, synergistic effect between plasma and thermal reaction is not anticipated even this high temperature. It is important to note that selectivity might be affected by high reaction temperature, but methane conversion falls fur short of equilibrium value in the absence of catalyst. On the other hand, nickel catalyst does not show catalytic activity below 400 °C, and methane conversion was half of the equilibrium value at 600 °C. If the temperature reached 700 °C, methane conversion abruptly increased and attained equilibrium value.

BEC reactor exceeded equilibrium conversion over the tested temperature range. The strong synergistic effect of barrier discharge and nickel catalyst was observed between 400 and 600 °C: methane conversion exceeded combined result of barrier discharge and nickel catalyst. On the other hand, catalytic reaction predominates over barrier discharges above 700 °C, and synergistic effect was not achieved below 200 °C. Methane conversion curve for Ni/SiO_2 shifted to 200 °C left in the presence of barrier discharges: this means that the apparent activation temperature for nickel catalyst seemed to be lowered due to the existence of barrier discharges. In addition, we did not observe carbon deposition in BEC reactor, even though $H_2O/CH_4 = 2$ was mostly maintained during the experiment.

Fig. 11(a) and (b) shows the product selectivity obtained by BEC reactor. When the temperature was 200 °C, reaction characteristics were very similar to those obtained by DBD reactor: 50% of carbonaceous products were C_2 (mainly ethane) and C_3 (propane) hydrocarbons. Product selectivity approaches equilibrium composition with increasing reaction temperature, and perfectly follows equilibrium curve over 600 °C. It is interesting to note that methane conversion largely exceeded equilibrium value, but products selectivity follows equilibrium one. This means that electron impact process plays an important role during gas phase methane activation: not only ground state methane molecule, but also excited molecule can be decomposed on nickel catalyst, leading to apparent low temperature activation of methane.

4.5. Energy cost and energy efficiency

There are many possible definitions to characterize energy cost of various reforming processes including conventional catalytic one. We first define energy efficiency with the specific formulae. The analysis was based on energy spent by DBD or BEC reactor. The power efficiency of high voltage power circuit, that is power spent by plasma reactor divided by plug-in power, was about 60%, and not included in this analysis. Fig. 12 shows the schematic diagram of enthalpy balance for a typical reformer. Most commonly accepted definition would be Eq. (3) that is expressed by higher heating

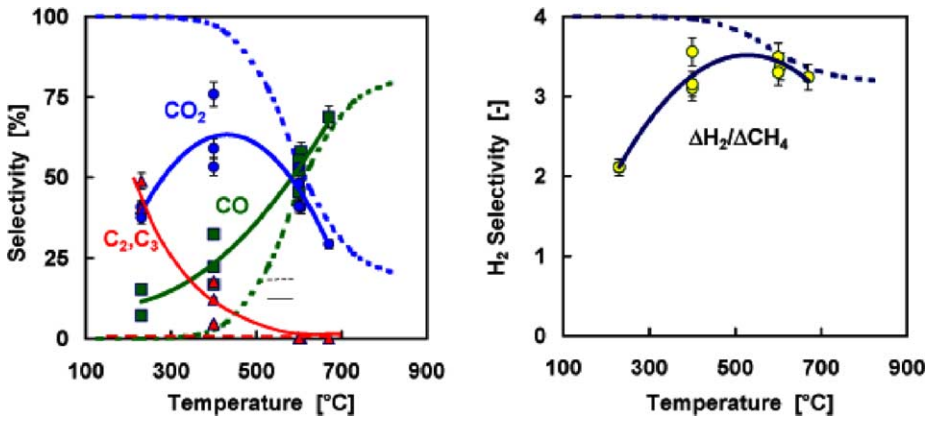

Fig. 11. Products selectivity of packed-bed barrier discharge reactor: (a) CO, CO_2, $C_2 + C_3$; (b) H_2. (- - -) equilibrium curve.

value of methane, syngas, and external enthalpy input:

$$\text{energy efficiency}\,(\%) = \frac{\Delta H_{\mathrm{CO}} + \Delta H_{\mathrm{H_2}}}{\Delta H_{\mathrm{CH_4}} + W} \times 100 \qquad (3)$$

Here $\Delta H_{\mathrm{H_2}}$ is the higher heating value of hydrogen (285.8 kJ/mol), ΔH_{CO} the carbon monoxide (283.0 kJ/mol), $\Delta H_{\mathrm{CH_4}}$ the methane (890.3 kJ/mol) and W the external energy input. The highest energy efficiency for modern catalytic reformer combined with heat recycling system is able to attain 90%. This means that at least 30% of initial methane must be completely combusted to provide high temperature heat source. In the case of plasma reforming, high energy electron must provide not only radical species, but also enthalpy required for endothermic reaction. Energy efficiency provided by DBD reactor was in the range of 5–20%, but BEC reactor reached as high as 69%. Table 3 compares the energy cost and energy efficiency at various reforming conditions.

Energy efficiency can be also defined by endothermic reaction enthalpy with respect to external energy input:

$$\text{energy efficiency}\,(\%) = \frac{\Delta H_{\mathrm{reform}}}{W} \times 100 \qquad (4)$$

Here $\Delta H_{\mathrm{reform}}$ is the endothermic reaction enthalpy due to steam reforming. This definition is only applicable to endothermic reactions. In addition, energy consumption per unit hydrogen mass is often used in plasma reforming [34]:

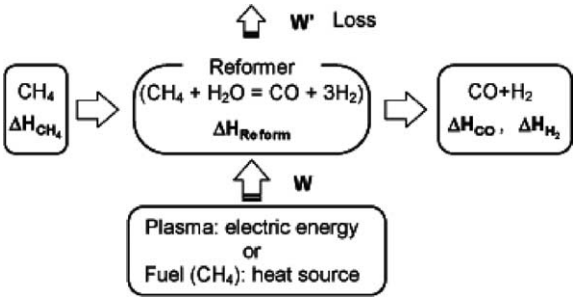

Fig. 12. Energy diagram.

$$\text{energy cost}\,(\mathrm{MJ/kg\,H_2}) = \frac{W}{[\mathrm{H_2}]} \qquad (5)$$

Here $[H_2]$ is the hydrogen mass production rate (kg/s). Energy cost for partial oxidation of methane using spark discharge is 267 MJ/kg H_2 (H_2 selectivity: 38%, CO selectivity: 65%). Steam reforming using gliding arc discharge achieved the highest value of 97 MJ/kg H_2 with CH_4 conversion of 44%. Energy efficiency defined by Eq. (4) was 33%. On the other hand, dry reforming using high temperature arc discharge resulted in 234 MJ/kg H_2 with 27% energy efficiency (Eq. (4)). All these plasma sources are considered as transient arc discharges. Electron temperature seems to be higher than gas temperature, but gas temperature is increased by several 100–1000 °C. Not only electron impact, but also high temperature heat source plays an important role during endothermic reforming processes. In this work, energy cost for BEC reactor operated at 600 °C and 10 kHz resulted in 136 MJ/kg H_2 with 88% hydrogen selectivity and 64% methane conversion. Energy cost and energy efficiency was effectively improved in plasma–catalyst combined reactor.

4.6. Energy regeneration from low temperature heat source via vibrationally excited methane

As previously mentioned, methane molecules excited to stretching vibrational state are about 1600 times more reactive on clean nickel surface than those in the ground state. In addition, computer simulation presented in Section 2 predicts that most abundant and long-lived radical species produced by electron impact is vibrationally excited methane: number density of those radical species reached 100 times higher than electron density and consumed 40% input electric energy. Reaction mechanism in relation to reaction temperature is discussed in detail in separate paper [35].

Fig. 13 schematically presents potential curve for methane molecule. Thermal dissociation of methane to H and CH_3, for example, follows the ground state potential curve. This process requires high temperature heat source (>800 °C) and consumed 4.26 eV dissociation energy. On the other hand,

Table 3
Comparison of energy cost and energy efficiency

Reaction type	Power (W)	Conversion (%)	Selectivity (%)		Energy efficiency and cost[a]		
		CH_4	H_2	CO	Eq. (3) (%)	Eq. (5) (MJ/kg H_2)	Eq. (4) (%)
I (DBD)							
200 °C, 10 kHz	15.3	13	53	34	21	5974	0.5
400 °C, 76 kHz	67.2	49	53	41	5	8080	0.4
III (DBD–Ni/SiO_2)							
400 °C, 10 kHz	3.29	10	51	2	61	1330	2.0
400 °C, 76 kHz	25.2	47	89	17	23	1004	3.3
600 °C, 10 KHz	4.40	64	88	40	69	*136*	26.5
600 °C, 76 kHz	28.7	87	84	58	22	691	5.3
IV (Ni/SiO_2)							
600 °C	–	33	94	21	–	–	–
General steam reformer (20 sccm at 800–900 °C)[b]	5.7	100	100	100	90	63	66

[a] Reaction enthalpy (endothermic) regarding C_2 and C_3 formation is not considered.
[b] Energy efficiency defined by Eq. (3) is assumed to be 90% with $CH_4 + H_2O = CO + 3H_2$.

methane dissociation by electron impact must follow upper electronic state that is expressed as dissociation curve since electric excitation takes place much faster than vibrational mode of nuclei. This is called well-known Franc–Condon principal. The great benefit of electronic process is that this process proceeds independently of temperature and pressure, but main drawback is that electrons have to lose much larger energy than dissociation energy (4.26 eV) by single collision. Excess energy fed into methane molecule increases kinetic energy of H and CH_3. Based on our numerical simulation, 50% of electric energy can be utilized for dissociation collision to form CH_i ($i = 0$–3) and H radicals. However, 60% of those excited energy must be used up for gas heating as an excess input energy: 30% of the input electric power is going to be wasted as excess energy input. This is the main reason that energy cost for plasma processes are much lower than that for thermal processes [36,37].

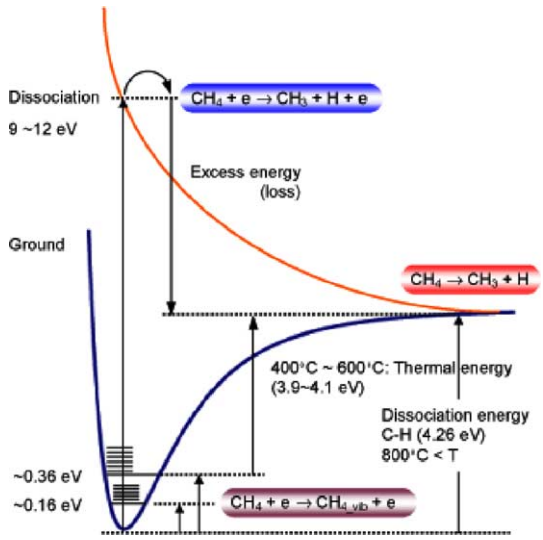

Fig. 13. Methane activation by thermal energy, electron impact, and their combined effect.

Plasma enhanced catalytic reaction is explained by two-step excitation as shown in the figure. Vibrational state of methane (bending mode: 0.16 eV, stretching mode: 0.36 eV) is produced by inelastic electron collision. Vibrational methane then dissociate at relatively lower temperature (400–600 °C). Although vibrational excitation energy only occupies 10% of the dissociation energy, this process greatly enhance chemical conversion processes at lower temperature. In addition, this kind of electronic process does not requires excess energy input since molecular excitation takes place within ground state potential curve. Plasma–catalyst reaction system is able to regenerate vibrational energy that was wasted in the absence of catalyst.

5. Conclusions

We developed barrier-discharge enhanced catalytic-bed (BEC) reactor for methane steam reforming, and successfully improved energy cost and energy efficiency. Some of the important aspects are as follows:

- DBD reactor
  1. Methane co5nversion monotonically increased with specific input energy. Various operating conditions such as gas composition, frequency, and temperature showed little impact on methane conversion and products selectivity.
  2. Forty percentage of methane converted to higher hydrocarbon such as ethane, propane, and butane. Hydrogen selectivity was 60% when specific input energy reached 10 eV/molecule.
- BEC reactor
  3. Methane conversion in plasma combined packed-bed reactor (3 wt.% Ni/SiO_2) exceeded equilibrium conversion over the temperature range between 400 and 600 °C: it exceeded combined conversion of barrier

discharge and catalyst. On the other hand, product selectivity tended to follow equilibrium composition.

4. Energy cost in BEC reactor achieved 136 MJ/kg H_2 with 88% hydrogen selectivity and 64% methane conversion at 600 °C and 10 kHz. The corresponding energy efficiency was 69% (Eq. (3)).
5. The apparent activation temperature for given nickel catalyst was lowered 200 °C in the presence of barrier discharge. This is probably because that vibrationally excited methane would improve dissociative chemisorption on nickel surface.
6. $H_2O/CH_4 = 2$ was applicable without carbon deposition on nickel surface. Vibrational excitation of H_2O must improve methane oxidation in plasma–catalyst combined reactor.

Acknowledgements

This research was partly supported by the Ministry of Education, Science, Sports and Culture, Grant-in-Aid for Young Scientists (B), 14750132, 2002, and The Mizuho Science Foundation. Authors also would like to thank Prof. M. Suzuki, Associate Prof. H. Akatsuka, Associate Prof. T. Watanabe, and Associate Prof. Y. Kato (all from Tokyo Institute of Technology) for intensive discussion.

References

[1] K. Okazaki, T. Nozaki, Therm. Sci. Eng. 7 (6) (1999) 109–114.
[2] K. Okazaki, T. Nozaki, Pure Appl. Chem. 74 (3) (2002) 447–452.
[3] K. Okazaki, T. Kishida, K. Ogawa, T. Nozaki, Energy Conv. Manage. 43 (2002) 1459–1468.
[4] B. Pietruszka, K. Anklam, M. Heintze, Proceedings of the 16th International Symposium on Plasma Chemistry (ISPC-16), Taormina, Italy, June 2003, p. 582.
[5] T. Hammer, T. Kappes, W. Schiene, in: C.J. Liu, R. Mallinson, M. Aresta (Eds.), Utilization of Greenhouse Gases, ACS Symposium Series No. 852, Section 6, No. 19, 2002.
[6] T. Kappes, W. Schiene, T. Hammer, Proceedings of the Eighth International Symposium on High Pressure Low Temperature Plasma Chemistry, Pühajärve, Estonia, July 21–25, 2002, pp. 196–200.
[7] H. Kabashima, H. Einaga, S. Futamura, IEEE Trans. Ind. Appl. 39 (2) (2003) 340–345.
[8] L.B.F. Juurlink, P.R. McCabe, R.R. Smith, C.L. DiCologero, A.L. Utz, Phys. Rev. Lett. 83 (4) (1999) 868–871.
[9] C.T. Ceyer, J.D. Beckerle, M.B. Lee, S.L. Tang, Q.Y. Yang, M.A. Hines, J. Vac. Sci. Technol. A 5 (4) (1987) 501–507.
[10] H. Burghgraef, A.P. Jansen, R.A. van Santen, J. Chem. Soc. 101 (12) (1994) 11012–11020.
[11] H.H. Kim, K. Tsunoda, S. Katsura, A. Mizuno, IEEE Trans. Ind. Appl. 35 (6) (1999) 1306–1310.
[12] H. Kim, A. Mizuno, Y. Sakaguchi, Energy and Fuels 16 (4) (2002) 803–808.
[13] A. Ogata, D. Ito, K. Mizuno, S. Kushiyama, T. Yamamoto, IEEE Trans. Ind. Appl. 37 (4) (2001) 959–964.
[14] T. Yamamoto, M. Okubo, K. Hayakawa, K. Kitaura, IEEE Trans. Ind. Appl. 37 (5) (2001) 1492–1498.
[15] S. Futamura, H. Einaga, A. Zhang, IEEE Trans. Ind. Appl. 37 (4) (2001) 978–985.
[16] T. Nozaki, Personal communication, 2002.
[17] W.L. Morgan, Plasma Chem. Plasma Process. 12 (4) (1992) 477–493.
[18] J. Davies, C.J. Evans, F. Llewellyn Jones, Proc. R. Soc. London Ser. A 281 (1964) 164–183.
[19] K. Tachibana, M. Nishida, H. Harima, Y. Urano, J. Phys. D 17 (1984) 1727–1742.
[20] S.K. Dhali, P.F. Williams, J. Appl. Phys. 62 (1987) 4691–4707.
[21] J. Li, S.K. Dhali, J. Appl. Phys. 82 (1997) 4205–4210.
[22] R. Morrow, L.E. Cram, J. Comp. Phys. 57 (1985) 129–136.
[23] R. Morrow, J. Comp. Phys. 43 (1981) 1–15.
[24] R. Morrow, T.R. Blackburn, K. Durbhakula, S. Dhali, IEEE Trans. Plasma Sci. 27 (1) (1999) 26–27.
[25] D. Braun, U. Kuchler, G. Pietsch, J. Phys. D 24 (1991) 564–572.
[26] D. Braun, V. Gibalov, G. Pietsch, Plasma Sour. Sci. Technol. 1 (1992) 166–174.
[27] V. Gibalov, D. Pietsch, Plasma Sour. Sci. Technol. 1 (2000) 166–174.
[28] M. Hayashi, in: L.C. Pitchford, et al. (Eds.), Swarm Studies and Inelastic Electron–Molecule Collisions, Springer-Verlag, Berlin, 1985, pp. 167–187.
[29] Y. Ohmori, K. Kitamori, M. Shimozuma, H. Tagashira, J. Phys. D 19 (1986) 437–455.
[30] L.M. Zhou, B. Xue, U. Kogelschatz, B. Eliasson, Energy and Fuels 12 (1998) 1191–1199.
[31] D.B. Hash, M. Meyyappan, J. Appl. Phys. 93 (1) (2003) 750–752.
[32] N.R. Franklin, H. Dai, Adv. Mater. 12 (2002) 890–894.
[33] O. Mutaf-Yardimci, A. Saveliev, A. Fridman, L.A. Kennedy, Int. J. Hydrogen Energy 23 (1998) 1109–1111.
[34] J.M. Cormier, I. Rusu, J. Phys. D 34 (2001) 2798–2803.
[35] T. Nozaki, N. Muto, S. Kado, K. Okazaki, Dissociation of vibrationally excited methane on Ni catalyst. Part 2. Process diagnostics by emission spectroscopy, Catal. Today, in press.
[36] T. Nozaki, Y. Miyazaki, Y. Unno, K. Okazaki, J. Phys. D 34 (23) (2001) 3383–3390.
[37] T. Nozaki, Y. Unno, K. Okazaki, Plasma Sour. Sci. Technol. 11 (2002) 431–438.